Journal of Alloys and Compounds 509 (2011) 5611–5616

Contents lists available at ScienceDirect

Journal of Alloys and Compounds

journal homepage: www.elsevier.com/locate/jallcom

Electrochemical fabrication of a porous nanostructured nickel hydroxide film electrode with superior pseudocapacitive performance

De-Shuai Kong[a], Jian-Ming Wang[a,*], Hai-Bo Shao[a], Jian-Qing Zhang[a,b], Chu-nan Cao[a,b]

[a] Department of Chemistry, Zhejiang University, Zheda Road 38#, Hangzhou 310027, PR China
[b] State Key Laboratory for Corrosion and Protection of Metal, Institute of Metal Research, Chinese Academy of Sciences, 62 Wencui Road, Shenyang 110016, PR China

ARTICLE INFO

Article history:
Received 15 November 2010
Received in revised form 16 February 2011
Accepted 17 February 2011
Available online 23 February 2011

Keywords:
Nickel hydroxide
Nanoporous structure
Pseudocapacitive performance
Dealloying
Electroplating
Electrochemical capacitors

ABSTRACT

A porous nickel film is prepared by selectively anodic dissolution of copper from an electrodeposited Ni–Cu alloy film. A porous nanostructured nickel hydroxide film electrode is further fabricated by the cathodic electrodeposition of $Ni(OH)_2$ film on the obtained porous nickel film. The specific capacitances of the as-prepared porous nanostructured $Ni(OH)_2$ film electrode at current densities of 2, 5 and 10 A/g are 1634, 1563 and 1512 F/g, respectively. The nanoporous Ni substrate significantly improves the electrochemically cyclic stability of the electrodeposited nickel hydroxide film in 1.0 M KOH solution. The superior pseudocapacitive properties such as large specific capacitance, excellent rate capability and improved electrochemically cyclic stability of the as-prepared nickel hydroxide electrode suggest its potential application in electrochemical capacitors.

1. Introduction

The electrochemical capacitors (ECs) have recently attracted increasing attention for use in high-power energy storages [1–5]. The energy stored in the ECs is either capacitive or pseudocapacitive in nature. The nonfaradaic double-layer capacitance is based on charge separation at the electrode/electrolyte interface [1,5]. The faradaic pseudocapacitance results from fast and reversible redox processes occurring at or near the solid electrode surface [6–10]. Hydrous ruthenium oxide has been reported to have remarkably high specific capacitance values (658–760 F/g), exhibiting ideal pseudocapacitive behavior [11,12]. However, the high cost of ruthenium limits its commercial application. Accordingly, the pseudocapacitive properties of inexpensive transition metal (Ni, Mn, Co, etc.) oxides or hydroxides have been explored [5,13–15].

Nickel hydroxide/oxide is considered as a promising electrode material for ECs due to its distinctive electrochemical properties. Various methods have been investigated to fabricate nickel hydroxide/oxide with superior capacitive performance. Techniques such as chemical precipitation [16], reactive radio-frequency sputtering [17], electrochemical deposition [6,12], and sol–gel processes [18] have been proposed. The typical specific capacitances of these nickel-based materials range from 50 to 350 F/g, depending on the preparation methods. However, the specific capacitances reported are still much lower than the corresponding theoretical values (2584 F/g for NiO and 2082 F/g for $Ni(OH)_2$ in a potential window of 0.5 V). This shows the limited electrochemical utilization of nickel hydroxide/oxide. Improvement on its specific capacitance is becoming a challenge.

It is well known that the properties of electrode materials can be significantly influenced by their specific surface area and morphologies [19–21]. The electrode material with high surface area and a uniform pore network of nanometer dimension would be expected to exhibit superior performance [22,23]. Among the existing synthetic approaches, electrochemical techniques show unique principles and flexibility in the control of the structures and morphologies of nanoporous film materials [12,13]. The main advantage of electrochemical techniques is the relatively facile control on the morphologies and microstructures of deposited films by changing deposition variables.

In this work, a porous nickel film is prepared by selectively anodic dissolution of copper from an electrodeposited Ni–Cu alloy film. A porous nanostructured nickel hydroxide film electrode is further fabricated by the cathodic electrodeposition of $Ni(OH)_2$ film on the obtained porous nickel film. The pseudocapacitive properties of the as-prepared porous nanostructured nickel hydroxide film electrode are evaluated and discussed.

2. Experimental

2.1. Electrode preparation

The Ni–Cu alloy film was prepared by the cathodic electrodeposition in the solution containing 1 M $NiSO_4$, 0.05 M $CuSO_4$ and 0.5 M H_3BO_3 [24,25]. The depo-

* Corresponding author. Tel.: +86 571 87952318; fax: +86 571 87951895.
E-mail address: wjm@zju.edu.cn (J.-M. Wang).

0925-8388/$ – see front matter © 2011 Elsevier B.V. All rights reserved.
doi:10.1016/j.jallcom.2011.02.086

sition process was conducted at room temperature in a three-electrode cell with a platinum counter electrode and a Ag/AgCl reference electrode. A stainless steel (SS) foil with an exposed area of 2.0 cm^2 was assembled as the working electrode. Prior to deposition, the SS foil was polished with 2000# grit waterproof abrasive paper, and ultrasonically cleaned in acetone and deionized water for 10 min, respectively. The alloy film was deposited at a constant potential of −0.8 V, and the total charges passed were controlled to be 6 C. Selective dissolution of Cu from the alloy film was conducted in the same solution by applying an anodic potential of 0.5 V until a cutoff current density of 10 μA/cm^2. Consequently, a porous nickel film was obtained. Nickel hydroxide film electrode was further fabricated by the cathodic electrodeposition of $Ni(OH)_2$ film on the obtained porous nickel film in a 0.01 M nickel nitrate aqueous solution. The electrodeposition was conducted at a current density of 1 mA/cm^2 for 4 min at room temperature (25 °C) in a three-electrode cell with a platinum counter electrode and a Ag/AgCl reference electrode [26]. Almost the same amount of nickel hydroxide was also deposited on a bare SS substrate to fabricate a comparable electrode.

2.2. Physical characterization

The morphologies of various thin film electrodes were examined by scanning electron microscopy (SEM, SIRION-100, FEI Co. Ltd.). The surface composition of the electrodes was analyzed by energy dispersive X-ray (EDX) spectroscopy (GENE IS 4000). The X-ray diffraction (XRD) patterns of the samples were recorded using a Rigaku D/Max 2550 X-ray diffractometer with Cu Kα radiation at 40 kV and 300 mA. The mass of nickel hydroxide was measured by a microbalance (Sartorius CP225D) with an accuracy of 0.01 mg.

2.3. Electrochemical tests

Electrochemical measurements were performed in a typical three-electrode glass cell with a platinum counter electrode and a Ag/AgCl reference electrode. Various film electrodes were used as the working electrode. 1.0 M KOH solution was employed as electrolyte. Cyclic voltammetry (CV) was conducted in a potential range of 0–0.6 V at various scan rates using a potentiostat (CHI 1140A). Galvanostatic charge/discharge tests were performed in a potential window of 0.5 V by a potentiostat (Arbin BT-2000, USA).

3. Results and discussion

The cyclic voltammograms of the SS electrode in the solution with 1 M $NiSO_4$, 0.05 M $CuSO_4$ and 0.5 M H_3BO_3 are illustrated in Fig. 1. In the potential region of −0.6 to 0.6 V (Fig. 1A), one reduction peak (c_1) representing the deposition of copper occurs at −0.28 V during the cathodic scan, and in the reverse scan, the corresponding oxidation peak (a_1) at ~0.2 V results from the stripping of the deposited copper [24]. It is noted that the integrated charges under the anodic peak are almost equal to those under the cathodic peak, suggesting that the deposited copper can be efficiently stripped. As shown in Fig. 1B, as the cathodic limit is extended to −1.0 V, a new cathodic peak occurs in the potential region of −0.70 to −1.0 V, which may be ascribed to the deposition of Ni [25]. In the reverse scan, a new anodic peak (a_2) occurs, which overlaps the anodic dissolution peak a_1 of pure Cu. The peak a_2 can be ascribed to the stripping of Cu from the Ni–Cu alloy formed during the cathodic deposition. The Ni oxidation peak is absent in Fig. 1B, resulting from the passivation of nickel [25]. The above CV results suggest that copper may be selectively dissolved from the Ni–Cu alloy.

As shown in Fig. 2a, new grains appear to form on previous ones during the electrodeposition, resulting in the columnar structure of the as-deposited alloy film [25]. Fig. 2b indicates that the phase segregation exists in the alloy film, with the active Cu-rich phases (the red regions) locating in the central parts of the columns and surrounded by the passive Ni-rich phases (the green regions), consistent with the previously reported results [24,25]. When the Ni–Cu alloy film is etched at 0.5 V, the Cu cores are selectively dissolved, and the Ni shells remain due to passivation. Thus a porous nickel film formed with hollow tubes (80–250 nm in diameter) is obtained, as shown in Fig. 3b. The obtained nanohollow tube structure is significantly different from the interconnected bicontinuous nanopores that are usually achieved by dealloying from a homogeneous binary solid solution alloy [27,28]. Fig. 3c exhibits the morphology of the deposited $Ni(OH)_2$ film on the porous Ni substrate. The granular $Ni(OH)_2$ with a nanosized diameter is perfectly deposited on the surface of the porous Ni film. The obviously narrowed pore size implies that some of $Ni(OH)_2$ grains are deposited into the nanopores. Accordingly, a nanostructured nickel hydroxide film electrode with high porosity is successfully achieved by the preceding electrochemical procedure.

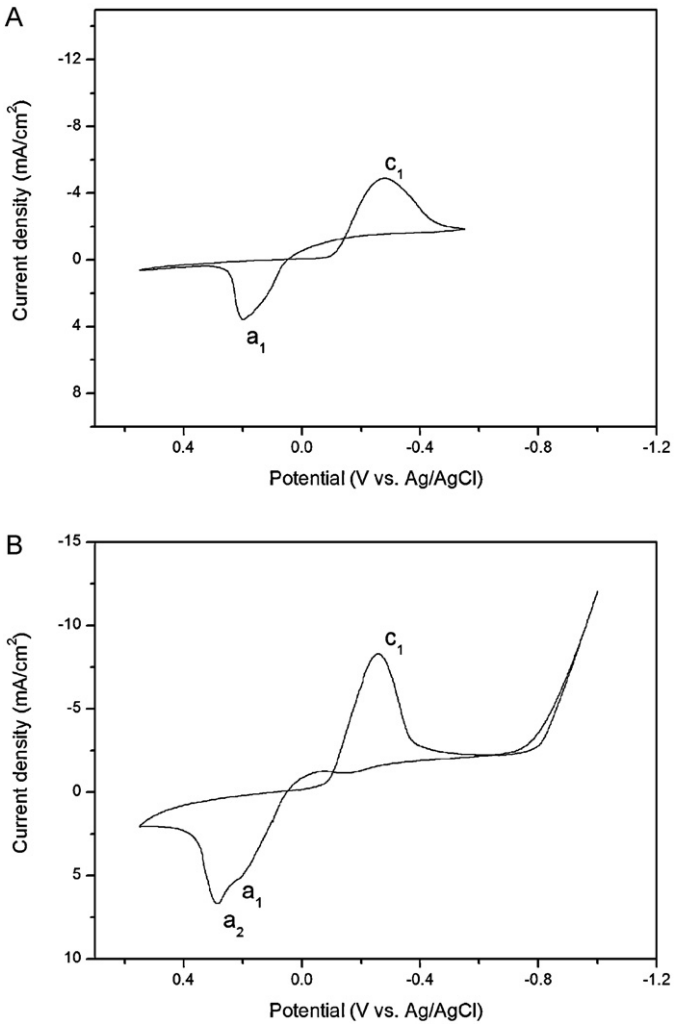

Fig. 1. Cyclic voltammograms of a SS electrode in the electrodeposition solution at a potential scan rate of 10 mV/s.

The XRD patterns of the same films as those in Fig. 3 are presented in Fig. 4. As shown in Fig. 4a, according to JCPDS files 04-850 and 04-836, all the peaks for the as-deposited alloy film result from metallic Ni and/or Cu. Although both Ni and Cu have a face-centered cubic (fcc) structure, the peak splitting in the diffraction pattern of the alloy film occurs in crystal planes (1 1 1), (2 0 0) and (2 2 0). This suggests the formation of inhomogeneous alloy with segregated Cu-rich and Ni-rich phases [25], consistent with the result in Fig. 2b. Fig. 4b shows that the diffraction peaks of Cu disappear, and those of Ni remain after the dealloying. This indicates that the nanoporous nickel film is obtained through uniform etching of copper from the alloy [24]. It is noted in Fig. 4c that a new peak at $2\theta = 34^\circ$ can be indexed to the (1 0 1) plane of α-$Ni(OH)_2$ according to JCPDS file 38-715, confirming the formation of α-phase $Ni(OH)_2$. Whereas the low intensity of the peak shows that the $Ni(OH)_2$ film on the surfaces of the nanoporous nickel film is thin.

The cyclic voltammograms of the as-prepared porous nanostructured $Ni(OH)_2$ film electrode are shown in Fig. 5. The surface faradaic reactions of $Ni(OH)_2$ film electrodes proceed according to

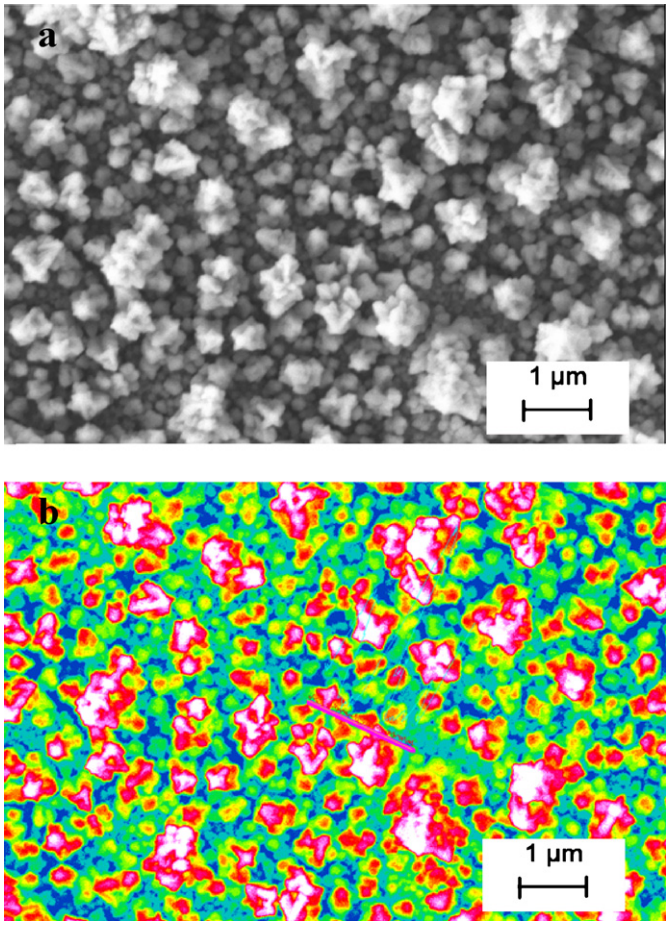

Fig. 2. (a) SEM image of the electrodeposited film and (b) EDX mapping of Ni and Cu elements in the film.

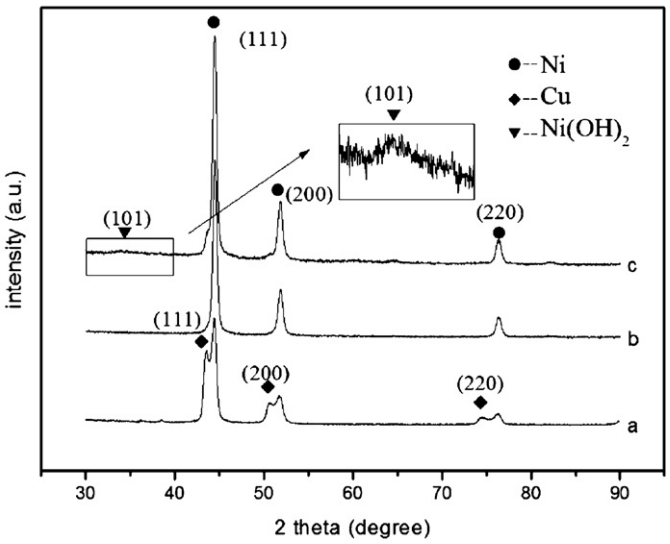

Fig. 4. XRD patterns of as-deposited alloy film (a), nanoporous film (b) and nanostructured $Ni(OH)_2$ film electrode (c).

the following reaction [6]:

$$Ni(OH)_2 + OH^- \leftrightarrow NiOOH + H_2O + e^- \quad (1)$$

As shown in Fig. 5a, the two strong redox peaks corresponding to oxidation/reduction of the $Ni(OH)_2$/NiOOH couple indicate the pseudocapacitive characteristic of the $Ni(OH)_2$ electrode. The symmetric characteristic of anodic charges and cathodic charges reveals the excellent reversibility of the electrode. In order to clarify the contribution of the nanoporous Ni substrate on the pseudocapacitance of the electrode, the CV curves of the bare porous Ni film and the nanostructured $Ni(OH)_2$ film electrode at a scan rate of 10 mV/s are compared in Fig. 5b. The occurrence of one couple of weak redox peaks in the CV curve of the bare porous Ni film implies

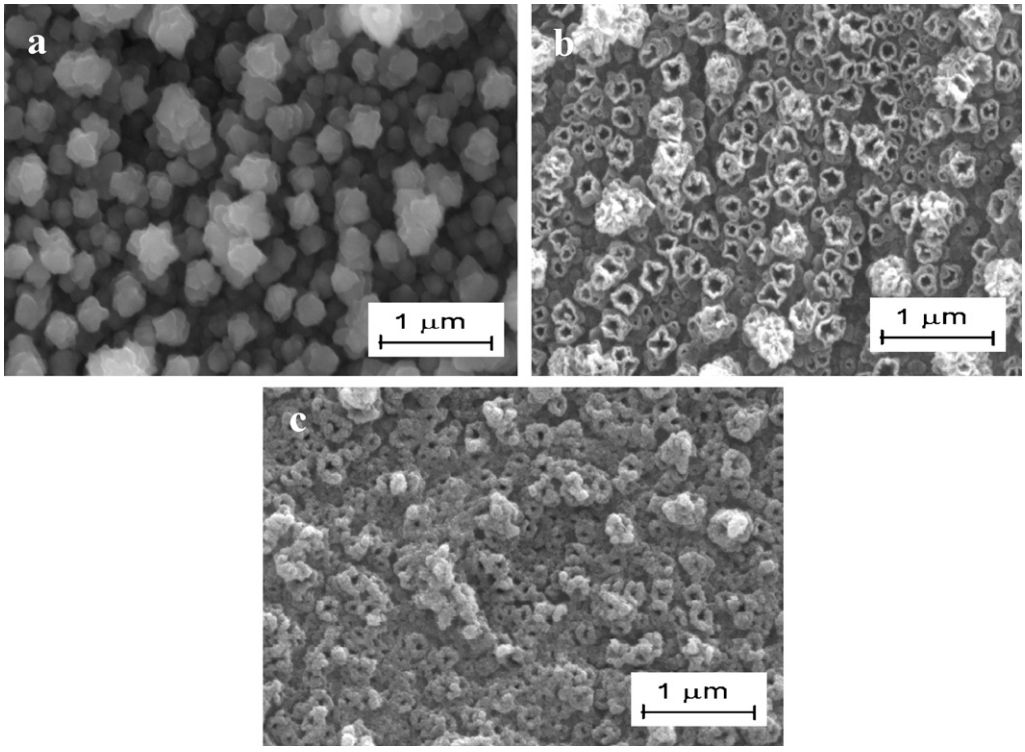

Fig. 3. SEM images of as-deposited Ni–Cu alloy film (a), nanoporous Ni film (b) and nanostructured $Ni(OH)_2$ film electrode (c).

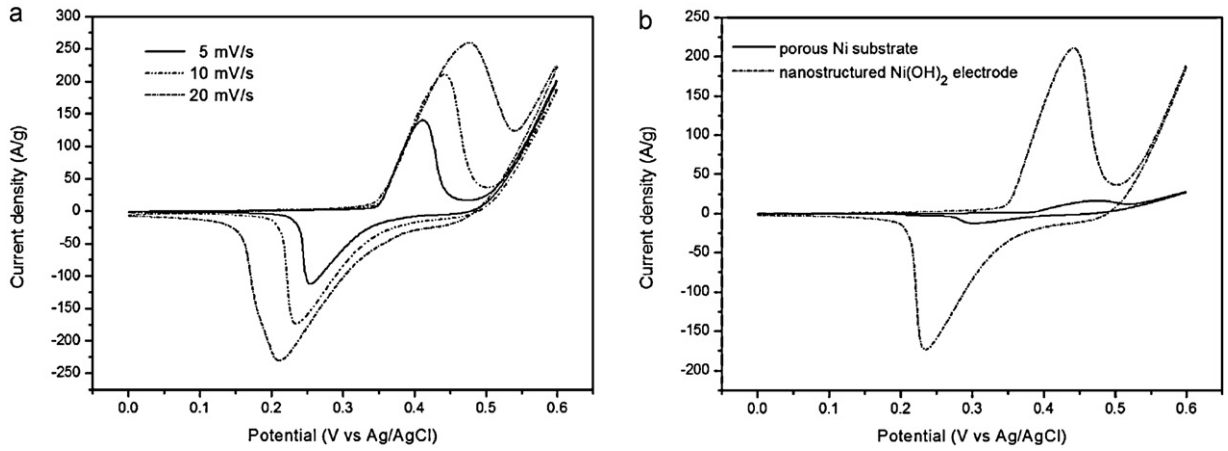

Fig. 5. (a) Cyclic voltammograms of as-prepared porous nanostructured $Ni(OH)_2$ film electrode at various scan rates and (b) cyclic voltammograms of porous Ni film and the nanostructured $Ni(OH)_2$ film electrode at a scan rate of 10 mV/s.

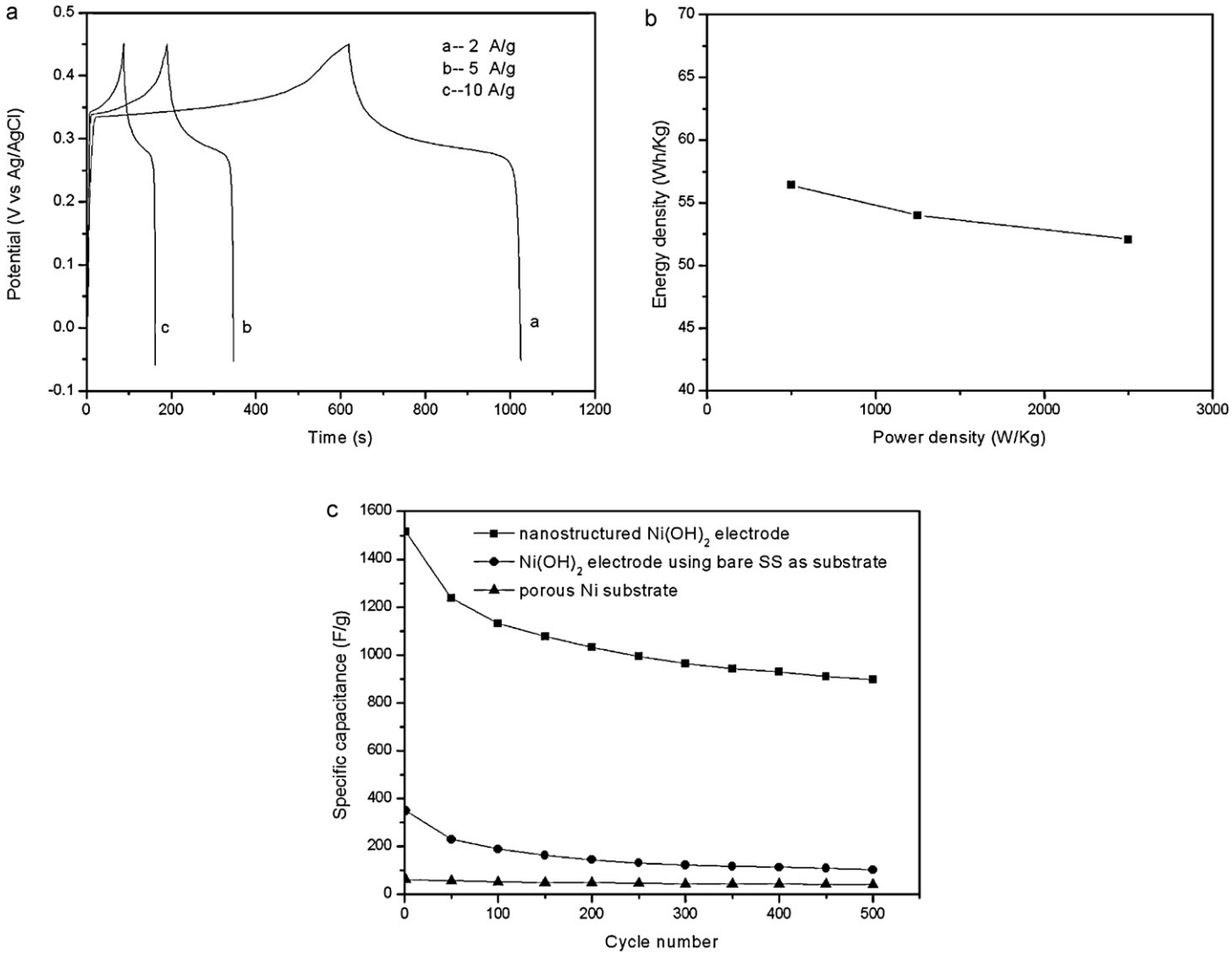

Fig. 6. (a) Galvanostatic charge–discharge curves of as-prepared porous nanostructured $Ni(OH)_2$ film electrode at various current densities, (b) Ragone plots of the nanostructured $Ni(OH)_2$ film electrode and (c) cyclic performance of the nanostructured $Ni(OH)_2$ film electrode, the $Ni(OH)_2$ film electrode using bare SS as substrate and the porous Ni substrate at a constant current density of 10 A/g.

its certain contribution to the pseudocapacitance [29]. However, the peak current for the porous Ni substrate is much lower than that for the $Ni(OH)_2$ electrode because only small amount of Ni hydroxide/oxide is formed on the nickel surface by passivation. This shows that the pseudocapacitance mainly results from the $Ni(OH)_2$ film.

Fig. 6a shows the galvanostatic charge–discharge curves of the as-prepared porous nanostructured $Ni(OH)_2$ film electrode at various current densities. All the curves exhibit one couple of obvious charge and discharge plateaus resulting from the transition between $Ni(OH)_2$ and NiOOH, indicating a typical pseudocapacitance behavior. This is consistent with the CV results in Fig. 5. The specific capacitance of an electrode during galvanostatic charge/discharge can be calculated by the following equation [30]:

$$C = \frac{i \cdot \Delta t}{m \cdot \Delta V} \quad (2)$$

where m is the mass of nickel hydroxide (g), ΔV is the potential window (V), and i is the discharge current (A) applied for time Δt (s). The specific capacitances of the porous nanostructured $Ni(OH)_2$ film electrode at current densities of 2, 5 and 10 A/g are 1634, 1563 and 1512 F/g, respectively. These specific capacitance values are much larger than those typical values previously reported [6,12,16–18,30]. The theoretical specific capacitance of $Ni(OH)_2$ for a 0.5 V potential window is 2082 F/g in terms of Eq. (1). The calculated utilization efficiency of the $Ni(OH)_2$ film electrode at a current density of 2 A/g is as high as 78%. The specific capacitance of the nanostructured $Ni(OH)_2$ film electrode at 10 A/g is as much as 93% of that at 2 A/g, suggesting its excellent rate capability. The high specific surface of the nanostructured $Ni(OH)_2$ film electrode may provide more active sites for the pseudocapacitive reaction. The nanoporous structure enhances the accessibility of KOH electrolyte and promotes reactive species transport within the electrode. The nanosized $Ni(OH)_2$ grains may shorten proton diffusion paths within the bulk of solid nickel hydroxide [5,31]. It is noted that the as-prepared $Ni(OH)_2$ is α phase (Fig. 4c), and α-$Ni(OH)_2$ transforms to γ-NiOOH on charging [32]. A larger specific capacity is expected for α-$Ni(OH)_2$/γ-NiOOH couple because the oxidation state of nickel in γ-NiOOH is 3.3–3.7 [33], compared with β-$Ni(OH)_2$/β-NiOOH couple. The above several points can be responsible for the relative high specific capacitance and excellent rate capability of the nanostructured $Ni(OH)_2$ film electrode.

The specific power density and specific energy density can be obtained by the galvanostatic charge–discharge curves in Fig. 6a [34,35]. The dependence of specific energy density on specific power density, which is labeled as the Ragone plot, is illustrated in Fig. 6b. Although the specific energy density generally decreases with increase in the specific power density, a low decrease value is observed. The nanostructured $Ni(OH)_2$ film electrode presents a specific energy density of 52.1 Wh/kg at a higher power density of 2500 Wh/kg, showing its potential application in electrochemical capacitors.

The cyclic properties of the as-prepared porous nanostructured $Ni(OH)_2$ film electrode, the $Ni(OH)_2$ film electrode using bare SS as substrate and the porous Ni substrate at a current density of 10 A/g are exhibited in Fig. 6c. The specific capacitance of the porous nanostructured $Ni(OH)_2$ film electrode gradually decreases in initial 200 cycles, and henceforth tends to level off with the electrochemical cycling. The nanostructured $Ni(OH)_2$ film electrode delivers a specific capacitance of 897 F/g after 500 cycles, showing a capacity retention of 59.3%. Although the capacitance retention is not high, the specific capacitance at the 500th cycle is much larger than those previously reported [6,16–18,30]. The nanostructured $Ni(OH)_2$ film electrode shows much larger specific capacitance than the $Ni(OH)_2$ film electrode using bare SS as substrate in all the investigated cycles. The capacity retention (59.3%) for the former is much higher than that for the latter (29.5%). This suggests that the nanoporous Ni substrate significantly improves the electrochemically cyclic stability of the electrodeposited nickel hydroxide film in 1.0 M KOH solution. It is noted that the bare porous Ni substrate presents much low specific capacitance in the electrochemical cycling. This further confirms that the $Ni(OH)_2$ film is mainly responsible for the high pseudocapacitance of the as-prepared porous nanostructured $Ni(OH)_2$ film electrode.

4. Conclusions

The porous nickel film formed with hollow tubes (80–250 nm in diameter) is obtained through the cathodic electrodeposition of Ni–Cu alloy film followed by selectively anodic dissolution of copper from the film. The porous nanostructured nickel hydroxide film electrode is successfully achieved by the cathodic electrodeposition of $Ni(OH)_2$ film on the obtained nanoporous nickel substrate. The as-prepared porous nanostructured $Ni(OH)_2$ film electrode presents a large initial capacitance of 1512 F/g and a high initial specific energy density of 52.1 Wh/kg at a relatively large current density of 10 A/g, and it still delivers a specific capacitance of 897 F/g after 500 cycles. The superior pseudocapacitive properties such as large specific capacitance, excellent rate capability and improved electrochemically cyclic stability of the as-prepared nickel hydroxide electrode can be attributed to its porous nanostructured characteristics and α phase structure. The present promising method may be also extended to fabrication of other nanostructured transition metal hydroxide/oxide electrodes.

Acknowledgement

This work was supported by National Natural Science Foundation of China (no. 50972128).

References

[1] J. Chmiola, G. Yushin, Y. Gogotsi, C. Portet, P. Simon, P.L. Taberna, Science 313 (2006) 1760–1763.
[2] A.S. Arico, P. Bruce, B. Scrosati, J.M. Tarascon, W.V. Schalkwijk, Nat. Mater. 4 (2005) 366–377.
[3] P. Simon, Y. Gogotsi, Nat. Mater. 7 (2008) 845–854.
[4] H. Adelkhani, M. Ghaemi, J. Alloys Compd. 493 (2010) 175–178.
[5] M.S. Wu, Y.A. Huang, C.H. Yang, J. Electrochem. Soc. 155 (2008) A798–A805.
[6] D.D. Zhao, W.J. Zhou, H.L. Li, Chem. Mater. 19 (2007) 3882–3891.
[7] L. Tian, A.B. Yuan, J. Power Sources 192 (2009) 693–697.
[8] M.S. Wu, M.J. Wang, J.J. Jow, J. Power Sources 195 (2010) 3950–3955.
[9] J. Zhang, L.B. Kong, J.J. Cai, H. Li, Y.C. Luo, L. Kang, Micropor. Mesopor. Mater. 132 (2010) 154–162.
[10] R.K. Dash, G. Yushin, Y. Gogotsi, Micropor. Mesopor. Mater. 86 (2005) 50–57.
[11] J.P. Zheng, P.J. Cygan, T.R. Jow, J. Electrochem. Soc. 142 (1995) 2699–2703.
[12] D.D. Zhao, S.J. Bao, W.J. Zhou, H.L. Li, Electrochem. Commun. 9 (2007) 869–874.
[13] M.S. Wu, M.J. Wang, Electrochem. Solid-State Lett. 13 (2010) A1–A3.
[14] V. Subramanian, H. Zhu, R. Vajtai, P.M. Ajayan, B. Wei, J. Phys. Chem. B 109 (2005) 20207–20214.
[15] L. Cao, F. Xu, Y.Y. Liang, H.L. Li, Adv. Mater. 16 (2004) 1853–1856.
[16] K.C. Liu, M.A. Anderson, J. Electrochem. Soc. 143 (1996) 124–130.
[17] S.H. Lee, C.E. Tracy, J.R. Pitts, Electrochem. Solid-State Lett. 7 (2004) A299–A301.
[18] Y.G. Wang, Y.Y. Xia, Electrochim. Acta 51 (2006) 3223–3227.
[19] Y.F. Liu, Y.H. Cao, L. Huang, M.X. Gao, H.G. Pan, J. Alloys Compd. 509 (2011) 675–686.
[20] U. Kasavajjula, C.S. Wang, A.J. Appleby, J. Power Sources 163 (2007) 1003–1039.
[21] J.Y. Xiang, X.L. Wang, X.H. Xia, J. Zhong, J.P. Tu, J. Alloys Compd. 509 (2011) 157–160.
[22] R.G. Lv, J. Yang, P.F. Gao, Y.N. NuLi, J.L. Wang, J. Alloys Compd. 490 (2010) 84–87.
[23] X.G. Wang, W.M. Wang, Z. Qi, C.C. Zhao, H. Ji, Z.H. Zhang, J. Alloys Compd. 508 (2010) 463–470.
[24] L. Sun, C.L. Chien, P.C. Searson, Chem. Mater. 16 (2004) 3125–3129.
[25] J.K. Chang, S.H. Hsu, I.W. Sun, W.T. Tsai, J. Phys. Chem. C 112 (2008) 1371–1376.
[26] D.A. Corrigan, R.M. Bendert, J. Electrochem. Soc. 136 (1989) 723–728.
[27] J. Erlebacher, M.J. Aziz, A. Karma, N. Dimitrov, K. Sieradzki, Nature 410 (2001) 450–453.

[28] Z. Qi, Z.H. Zhang, H.L. Jia, Y.J. Qu, G.D. Liu, X.F. Bian, J. Alloys Compd. 472 (2009) 71–78.
[29] C.T. Hsieh, Y.W. Chou, W.Y. Chen, J. Solid State Electrochem. 12 (2008) 663–669.
[30] S. Hosogai, H. Tsutsumi, J. Power sources 194 (2009) 1213–1217.
[31] M.S. Wu, Y.A. Huang, J.J. Jow, W.D. Yang, C.Y. Hsieh, H.M. Tsai, Int. J. Hydrogen Energy 33 (2008) 2921–2926.
[32] H. Chen, J.M. Wang, T. Pan, Y.L. Zhao, J.Q. Zhang, C.N. Cao, J. Power Sources 143 (2005) 243–255.
[33] Y.L. Zhao, J.M. Wang, H. Chen, T. Pan, J.Q. Zhang, C.N. Cao, Electrochim. Acta 50 (2004) 91–98.
[34] W. Xiao, H. Xia, J.Y.H. Fuh, L. Lu, J. Electrochem. Soc. 156 (2009) A627–A633.
[35] P.K. Nayak, N. Munichandraiah, Electrochem. Solid-State Lett. 12 (2009) A115–A119.